

Article

Effects of Laser Microtexturing on the Wetting Behavior of Ti6Al4V Alloy

Juan Manuel Vazquez-Martinez *, Jorge Salguero Gomez , Pedro Francisco Mayuet Ares, Severo Raul Fernandez-Vidal and Moises Batista Ponce

Department of Mechanical Engineering & Industrial Design, Faculty of Engineering, University of Cadiz, Av. Universidad de Cadiz 10, E-11519 Puerto Real-Cadiz, Spain; jorge.salguero@uca.es (J.S.G.); pedro.mayuet@uca.es (P.F.M.A.); raul.fernandez@uca.es (S.R.F.-V.); moises.batista@uca.es (M.B.P.)

* Correspondence: juanmanuel.vazquez@uca.es; Tel.: +34-956-483-513

Received: 20 March 2018; Accepted: 14 April 2018; Published: 17 April 2018



Abstract: Surface modification procedures by laser techniques allow the generation of specific topographies and microstructures that enable the adaptation of the external layers of materials for specific applications. In laser texturing processes, it is possible to maintain control over the microgeometry and dimensions of the surface pattern through varying the processing parameters. One of the main areas of interest in the field of surface modification treatments is the ability to generate topographies that are associated with specific surface finishes, in terms of roughness, that can improve the manufactured part's functional capabilities. In this aspect, several types of phenomena have been detected, such as the friction and sliding wear behavior or wetting capacity, which maintain a high dependence on surface roughness. In this research, surface texturing treatments have been developed by laser techniques through using the scanning speed of the beam (V_s) as a control parameter in order to generate samples that have topographies with different natures. Through assessments of surface finish using specialized techniques, the dimensional and geometrical features of the texturized tracks have been characterized, analyzing their influence on the wetting behavior of the irradiated layer. In this way, more defined texturing grooves has been developed by increasing the V_s , which also improves the hydrophobic characteristics of the treated surface. However, due to the lack of uniformity in the solidification process of the irradiated area, some deviations from the expected trends and singular points can be observed. Using the contact angle method to evaluate the wetting behavior of the applied treatments found increases in the contact angle values for high texturing speeds, finding a maximum value of 65.59° for $V_s = 200$ mm/s.

Keywords: surface engineering; laser texturing; wetting behavior; Ti6Al4V; surface characterization; roughness parameters

1. Introduction

The wetting features of a surface can improve the functional performance of manufactured parts in a wide field of applications, such as turbine blades or biomechanical components [1–6]. In the aeronautical and aerospace industry, the decrease of microdroplets on the surface of assembled components can reduce corrosive effects in environments associated with high relative humidity. On the other hand, the liquid absorption capacity allows adaptations to the wear properties of a surface under friction conditions when lubricants or cooling products are used [1,3,7–10]. Furthermore, the ability to maintain control over the wetting properties of a surface can produce benefits regarding the biocompatibility and biomechanical behavior of materials in relation to its cellular adhesion, or improving the sliding features under biological fluids situations in medical prostheses [9–13]. In the case of strategic material alloys for the aerospace industry and biomechanical applications such as

Ti6Al4V titanium alloy, surface modification treatments and evaluations are used to overcome material limitations and improve the functional performance of the alloy [9,12,14–20].

Although there are a wide range of modification treatments by chemical and mechanical procedures to adapt the surface to specific conditions, some treatments such as knurling can generate mechanical stress, and in other cases surface contamination, or result in variations of the properties in the inner layers of the alloy. In this aspect, surface texturing treatments using laser techniques allow the generation of topographies with microgeometry, and properties that are adapted to specific working conditions, without affecting the deeper layers of the material [14,16–26].

Previous research describes a direct relationship between the surface finish, in terms of roughness, and the wetting properties (contact angle) on a surface [27–30]. In this way, the Wenzel theory of the contact angle [29,31,32] describes the S_{dr} (developed interfacial area ratio) hybrid roughness parameter [33], and shows its important role regarding the wetting capacity of rough surfaces. The developed interfacial area ratio parameter describes the relationship between areas of a rough surface and the projected area of a flat surface [33].

The main objective of this research is focused on the study of the wetting behavior of Ti6Al4V titanium alloy surfaces textured by laser. For that reason, the surface finish and its influence on the contact angle of drops over the modified surface has been taken as the control variable.

2. Materials and Methods

2.1. Laser Texturing Process

Experimental procedures were carried out on UNS R56400 (Ti6Al4V) titanium alloy samples with 5.0-mm thickness. Test probes were conditioned by a mechanical grinding/polishing process using 1200 grits (particles per square inch) abrasive sandpaper, with the aim of obtaining a surface finish with the roughness parameters of $Ra < 0.05 \mu\text{m}$ and $Rz < 0.15 \mu\text{m}$. After the polishing process, all of the samples were cleaned using a petroleum ether 50% solution where the test probes have been submerged, removing polishing residues. With these initial conditions, laser texturing treatments have been developed using a $1070 \pm 5 \text{ nm}$ wavelength Ytterbium fiber infrared pulsed laser, model Rofin EasyMark F20 system (ROFIN-SINAR Technologies Inc., Plymouth, MI, USA), with a $60\text{-}\mu\text{m}$ spot diameter and 100-ns pulse width. Texturing treatments have been performed over Ti6Al4V samples in an open-air atmosphere through a bidirectional layout without overlapping, resulting in parallel irradiated lines with a separation of approximately 0.1 mm between laser tracks. Under these starting conditions, significant variations were set in the scanning speed of the laser beam (V_s), resulting in seven different tested surfaces with same pulse energy (E_t), fluence/energy density of the pulse (E_d), and changing the scanning speed (V_s). The laser-irradiated conditions of the texturing process are shown in Table 1.

$$E_T[\text{J}] = \frac{P[\text{W}]}{f[\text{Hz}]} \quad (1)$$

$$E_d \left[\frac{\text{J}}{\text{cm}^2} \right] = \frac{E_T[\text{J}]}{A_{\text{spot}} [\text{cm}^2]} \quad (2)$$

Table 1. Laser processing parameters.

P (W)	f (Hz)	E_T (mJ)	E_d (J/cm ²)	V_s (mm/s)						
				V_1	V_2	V_3	V_4	V_5	V_6	V_7
20	80,000	0.125	4.42	10	20	40	80	100	150	200

The textured probe presents seven surface conditions that range from higher intensity treatments at low scan speeds (Treatment 1), to less aggressive treatments with high V_s (Treatment 7), and compares the results with an untreated reference specimen (Treatment 8), Figure 1.

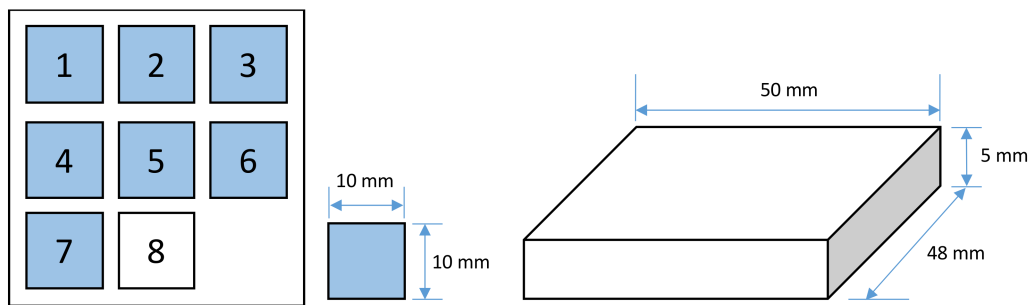


Figure 1. Dimensions and layout of textured samples.

2.2. Microgeometrical Evaluation of Laser Textured Probes

The characterization of the textured samples has been focused on the evaluation of the dimensional and geometrical features of the topography that result from each surface modification treatment by laser. This emphasis is in line with the main objective of this work, which is to obtain a first approach to a dependence relationship between the laser processing parameters and the surface finish in terms of the roughness and wetting behavior of the Ti6Al4V titanium alloy. For this purpose, the measurement of the surface finish in terms of the two-dimensional (2D) and three-dimensional (3D) roughness has been carried out through the measurement of the R_z , R_{Sm} , and S_{dr} parameters using a roughness measure station Mahr Perthometer Concept PGK120 (Mahr technology, Göttingen, Germany) for the 2D parameters, and an optical profiler Zeta Instruments, model Z-300 (Zeta-KLA-Tencor Company, Milpitas, CA, USA) for the measurement of the S_{dr} parameter.

Evaluation of the R_z and R_{Sm} parameters were performed by contact measurement following a perpendicular direction to the irradiated grooves. In order to complete the inspection of the surface texturized tracks, scanning electron microscopy (SEM) has been used. In this aspect, undetectable features have been detected at the surface level through the shape of the radiation grooves. Also, irregular cooling process has been observed in some cases, resulting in the deposition of material over the surface of the laser tracks. Therefore, it is difficult to detect the complete geometry of the material removed grooves. With the aim of studying the complete shape of the traces more accurately, cross-sections of the texturing layout have been analyzed.

2.3. Wetting Behavior of Laser Textured Probes

The evaluation of the wetting behavior of the textured surfaces has been carried out by measuring the contact angle between the solid and liquid phases through using a system formed by a volumetric pump, for the dosage of drops with specific size, a support platform for the positioning of samples, and a high resolution CCD camera located in front of a specific illumination system. This measuring system enables the evaluation of the contact angle between the drop and the textured surface. Contact angle measurements have been conducted in a perpendicular direction to the laser grooves. Samples have been evaluated in a period of time less than 1 h from the irradiated stage. During the entire measurement process, a temperature between 20–25 °C has been established.

3. Results and Discussion

3.1. Surface Finish (Roughness)

The roughness of the textured samples is one of the main control parameters for the study of the surface wetting capacity. The variations in the scanning speed result in a wide range of topographies with special characteristics. Through changes in the scanning speed of the beam, it is possible to increase or decrease the energy density, giving place to surfaces with different microgeometrical dimensions, as shown in Figure 2.

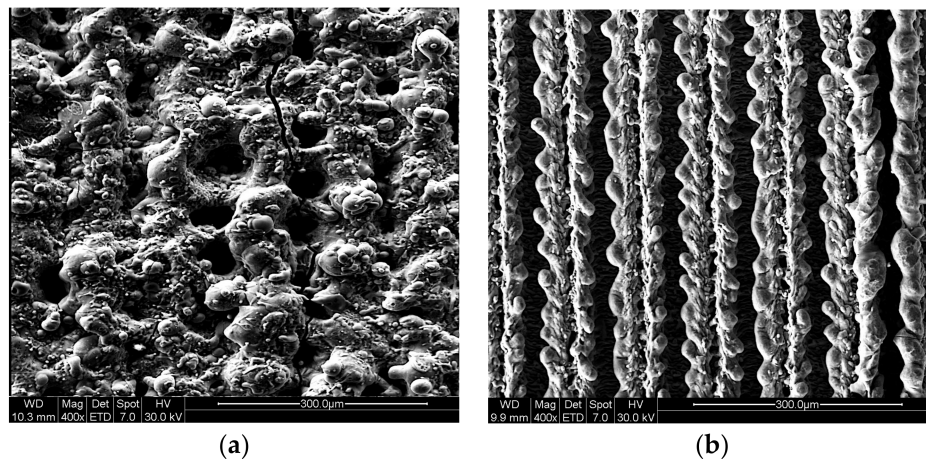


Figure 2. Surface topographies' evolution as a function of the scan speed of the beam (a) $V_s = 10$ mm/s; (b) $V_s = 200$ mm/s.

For low scanning speeds ($V_s = 10$ mm/s), the volume of vaporized material is very high in relation to the separation between the parallel textured lines, which overlap the bidirectional trajectories, and give rise to a less ordered topography than the high scanning speeds ($V_s = 200$ mm/s). This can be verified through the roughness induced by the surface modification treatment.

By analyzing the behavior of the Rz and RSm roughness parameters [34], a first approach to the material trends can be obtained through the variables relating to the maximum height of the profile and the spacing between peaks, favoring a first description of the traces produced by the laser treatment. The increase in V_s results in a decrease in the dimensions of the texturing tracks, mainly since the laser beam spends less time on the same section of the material. A decrease in the values obtained can be detected for the measurement of the maximum height of the profile and spacing of the peaks' roughness parameters, as shown in Figure 3. Also, it is noteworthy that the roughness values were obtained under conditions of low speed, in which a non-uniform trend is observed, especially due to a greater volume of melted material and instabilities in the cooling process. On the other hand, a significant decrease in the values of Rz and RSm has been detected for $V_s = 150$ mm/s. In this case, the presented roughness parameters behavior comes from the formation of solidified material debris on the surface of the textured groove, promoting a reduction in the size, in terms of the microgeometry, of the laser traces. The phenomena described will be discussed in a later section, which focuses on the evaluation of the groove geometry.

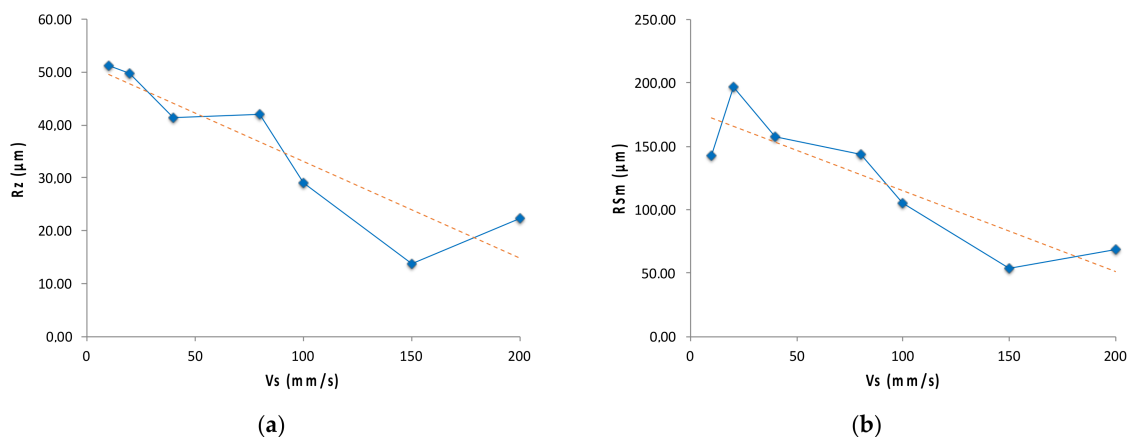


Figure 3. Surface finish behavior as a function of the scanning speed of the beam; (a) Rz and (b) RSm .

3.2. Shape of Irradiated Grooves

The geometry and dimensions of the traces produced by the laser beam are highly influenced by the selected treatment parameters. Likewise, more aggressive thermal procedures, which are controlled by low scan speed of the beam, result in a higher energy density supplied by the laser system. These processed conditions develop deep and thin textures, with a lack of uniformity in the surface, due to the unification of the contiguous lines of the beam track. As can be expected, the increase in scanning speed induces less aggressive treatments, leading to a significant decrease in the depth of material removed by the texturing process, as shown in Figure 4.

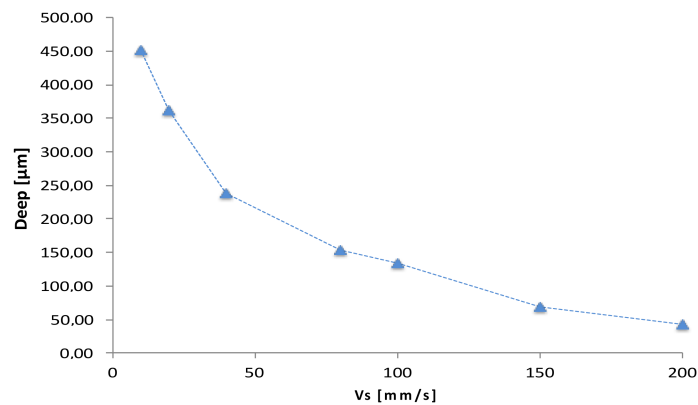


Figure 4. Maximum depth of grooves in textured samples.

On the other hand, variability in the shape of the texturing tracks can be observed, from sharper and deeper geometries to smoother topographies with semicircular grooves. However, the energy supplied by the laser plays an important role in the cooling stage of the melted metal. In this sense, the vaporization of the treated metal can be detected for lower scanning speeds; furthermore, for increases of V_s , solidification of the melted material along and over the surface of the textured surface is caused, as shown in Figure 5.

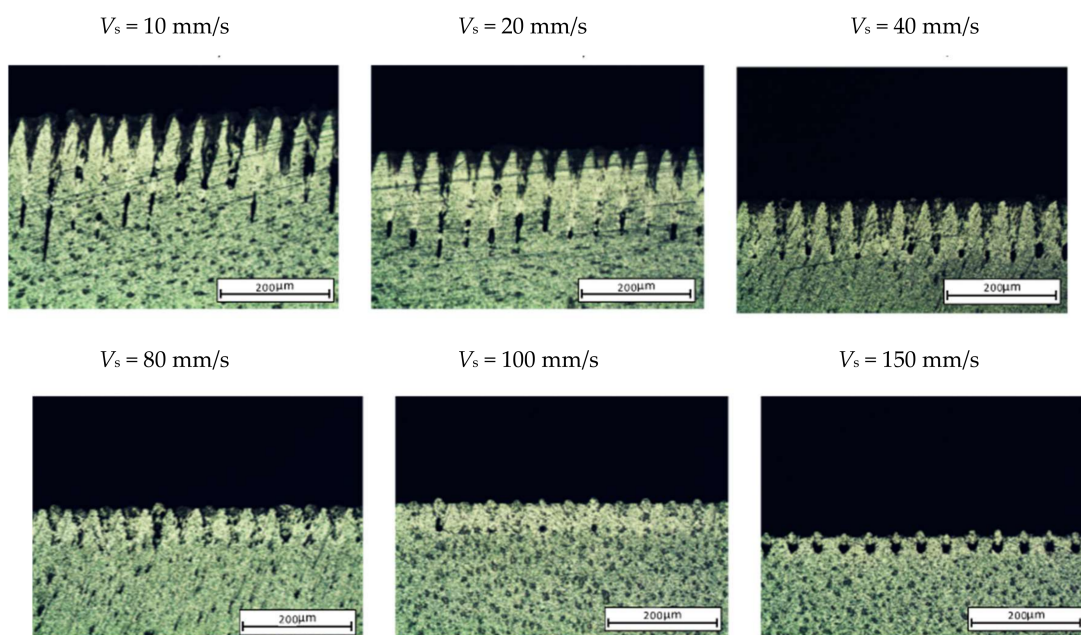


Figure 5. Cont.

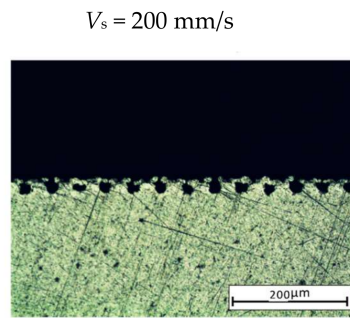


Figure 5. Evolution of texturized grooves geometry as a function of V_s .

It is noteworthy that for the intermediate values of the scan speeds (100–150 mm/s), a phenomenon whereby the melted material solidifies takes place in the surface area of the texturized grooves, causing a total or partial obstruction of the textured track ways. Due to this, variations in the previously mentioned expected values of roughness can be detected, causing alterations in other parameters, such as the wetting behavior of the surface, as shown in Figure 6.

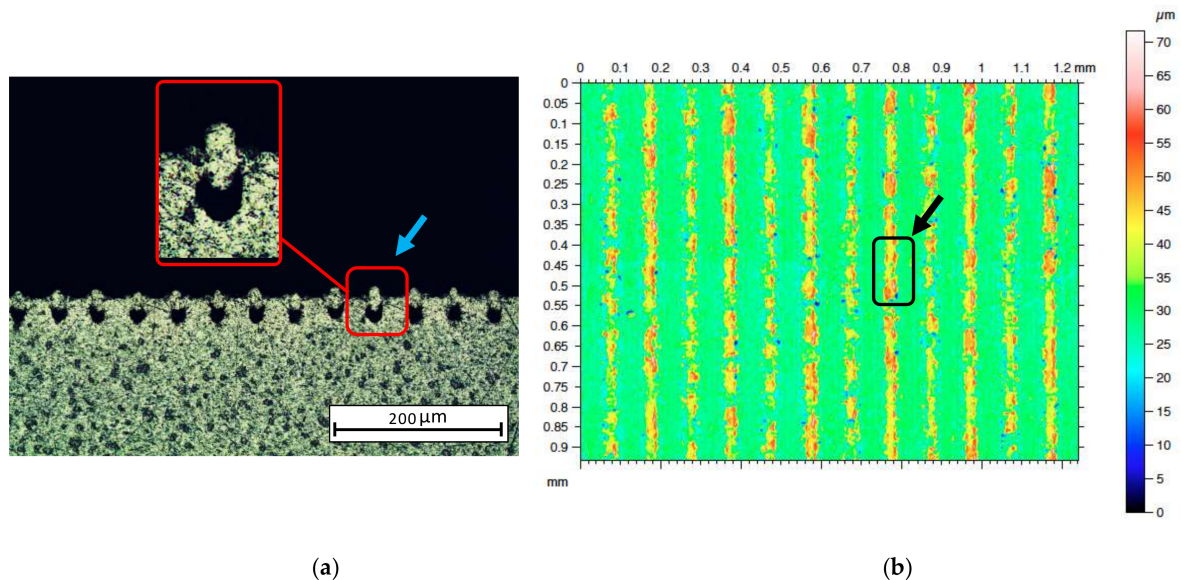


Figure 6. Solidification of melted metal over the textured grooves ($V_s = 150 \text{ mm/s}$). (a) Groove geometry; (b) Textured tracks height.

3.3. Wetting Behavior of Textured Surface

The wetting properties of a surface are usually evaluated through the contact angle between liquid and solid phases. In the case of rough surfaces, the Wenzel humectant model assumes that the drop of liquid penetrates the asperities, i.e., the liquid phase is introduced through the grooves formed by the roughness, as shown in Figure 7.

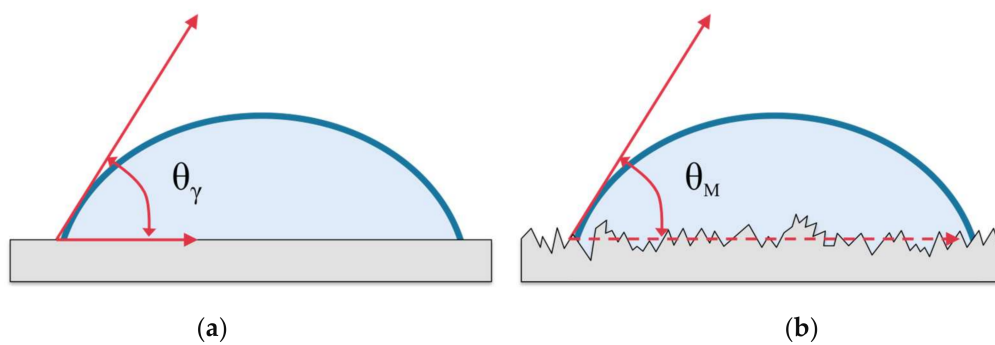


Figure 7. Wenzel model contact angle: (a) Flat surface; (b) Rough surface.

The Wenzel model describes a relation between the contact angle, the phases, and the surface roughness. For that, the roughness factor concept is developed as a proportionality coefficient between the contact angles of an ideal flat surface and a rough surface with asperities:

$$\cos\theta_m = r \cdot \cos\theta_Y \quad (1)$$

where θ_m is the value of the contact angle for the rough surface, θ_Y is the value of the contact angle of the Young's modulus for ideal flat surfaces, and r is the roughness factor.

In this way, the r roughness coefficient [34] is determined by the developed interfacial area ratio roughness parameter (Sdr). The Sdr 3D roughness parameter describes the ratio between the projected area and the rough area (subject to the texturing process) of the solid surface on which the liquid drop is deposited for the measurement of the contact angle. In this case, the Sdr parameter indicates a relation between the increment of surface contributed by the rough surface texture in respect to a surface without roughness:

$$Sdr = \frac{1}{A} \left[\iint_A \left(\sqrt{1 + \left(\frac{\partial z(x,y)}{\partial x} \right)^2 + \left(\frac{\partial z(x,y)}{\partial y} \right)^2} - 1 \right) dx dy \right] \quad (2)$$

Once the surface texture ratio is determined, the “ r ” roughness coefficient of the Wenzel model can be obtained as a function of the roughness area relation [35]; thereby, the wetting properties can be related to microgeometrical variations as a consequence of the V_s laser processed parameter.

$$r = 1 + \frac{Sdr}{100} \quad (3)$$

However, unexpected situations can be found in which the microgeometric features of the surface result in significant variations regarding the contact angle measurement between the calculated value and the real value of the textured surfaces. Significant dependence has been detected between the contact angle and the laser scanning speed of the beam of the textured surfaces, as shown in Figure 8a. This is mainly due to the development of well-defined and structured topographies for less aggressive treatments against laser treatments with lower V_s , in which a greater amount of energy is supplied.

Higher energy treatments (with lower V_s values) may cause the overlapping of parallel beam track lines, resulting in a lack of homogeneity across the textured surface. These phenomena can be the main reason for the observed decrease in contact angle values, favoring liquid absorption from the surface. On the other hand, the behavior of the values of the r coefficient, as a function of the V_s , shows a decreasing tendency when the scan speed is increased, as shown in Figure 8b.

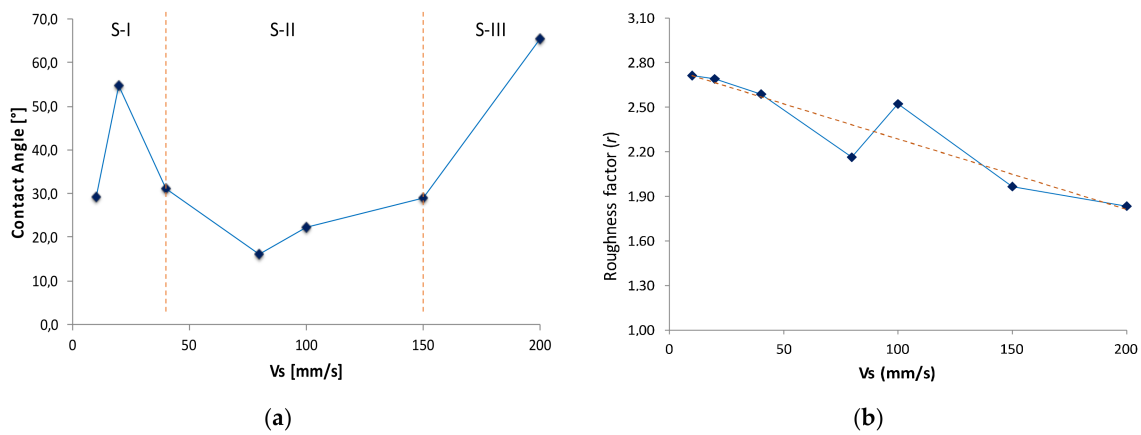


Figure 8. Wetting behavior as a function of the scanning speed of the beam’s (a) contact angle and (b) roughness coefficient.

The analysis of the results obtained for the study of the wettability properties, by means of the contact angle measurement, shows the existence of three well-differentiated sets/ranges of V_s in which different behaviors can be observed, especially due to the volume of melted material and the solidification process in the cooling phase.

For lower scanning speeds (S-I), as seen in Figure 8, a non-uniform evolution of wetting capacity is produced. An important increase has been detected in the compactness of the textured surface for $V_s = 20$ mm/s, where a layer with low values of roughness is generated from molten metal. Asperities with similar height are shown to be evenly distributed over the entire surface, presenting porosity in the texturing track lines.

Irradiated microgeometry favors the increase in the contact angle of the droplets that are deposited on the surface. On the other hand, the isolated growth of the asperities in irregular positions can be observed for 10 mm/s and 40 mm/s scanning speeds. A non-uniform arrangement of elements may cause a decrease in the surface compactness that is generated by laser texturing, favoring the loss of the surface tension of the drops and resulting in a reduction of the contact angle, as shown in Figure 9.

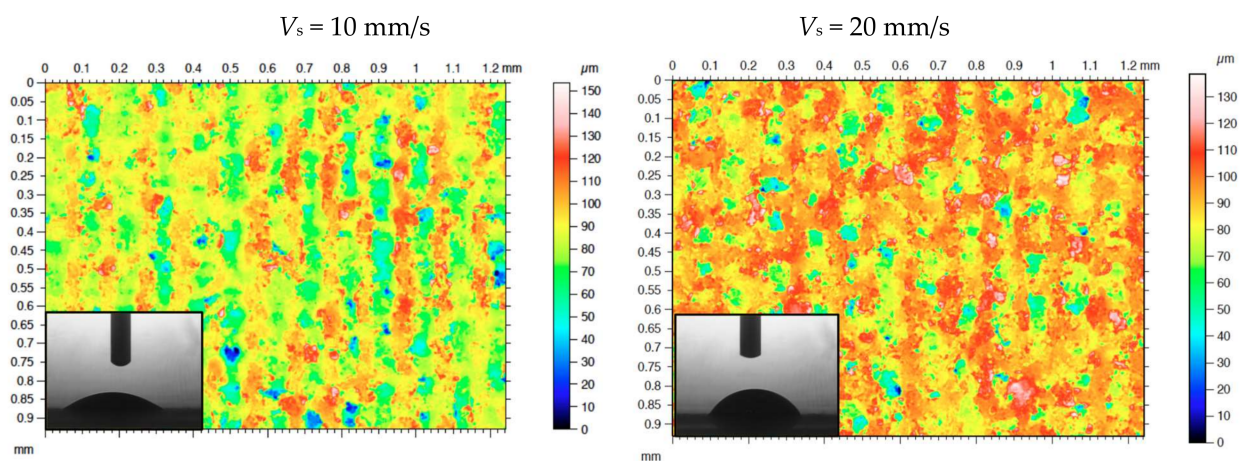


Figure 9. Cont.

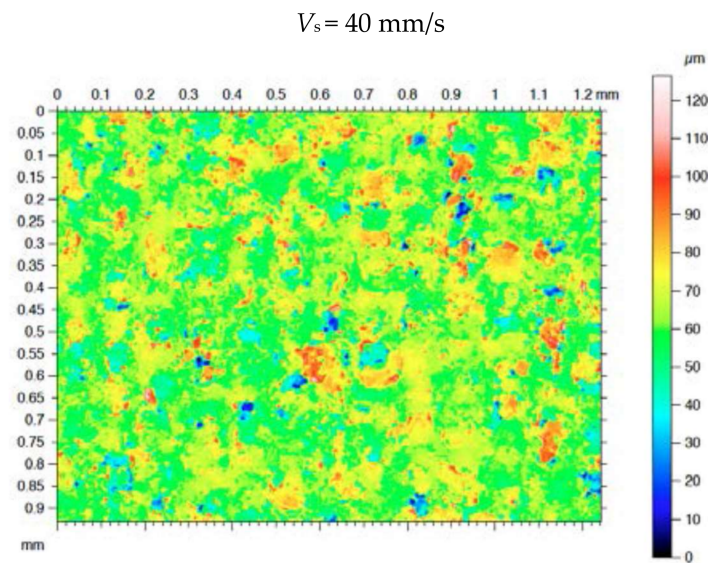


Figure 9. Topographic evolution of the textured layer for the S-I speed set, which has lower scanning speeds ($V_s = 10 \text{ mm/s}$ to $V_s = 40 \text{ mm/s}$).

In an intermediate speed range (S-II), a decrease in the fluctuations of the contact angle values is shown. For the scanning speed values between 40–150 mm/s, a growth of asperities in isolated positions can be observed; these are generated by instabilities in the cooling process, as seen in Figure 10. These phenomena may be the main cause of the decrease in the compactness of the treated layer, favoring the breaking of the surface tension of the drop on the surface, and resulting in contact angle attenuation values lower than 20° . In this regard, a change in trend has been detected in the contact angle values for $V_s = 100 \text{ mm/s}$, which coincides with a growth in the solidified material structures that obstruct the grooves; this growth was formed by the materials that were removed from the irradiated process. Such structures can grow randomly, as determined by lack of homogeneity of the cooling processes in the vaporization of the material and its subsequent deposition in the edges of the laser processing track. For $V_s = 100 \text{ mm/s}$, and coinciding with Figure 8b, a growth of protuberances has been detected in places where the laser pulses have impacted, increasing the area of the modified surface with respect to the projected surface, and thereby increasing the r roughness coefficient value.

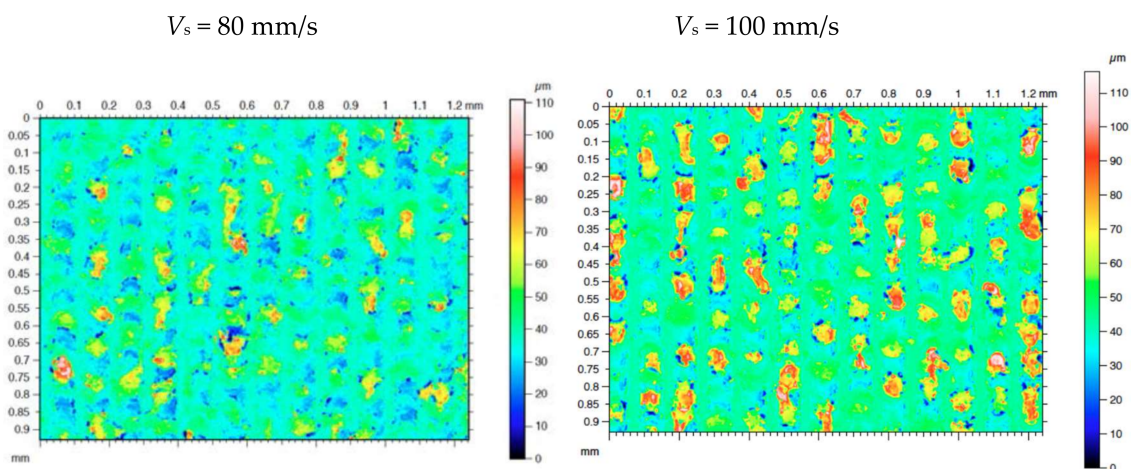


Figure 10. Topographic evolution of the textured layer for the S-II speed set, which has intermediate scanning speeds ($V_s = 80 \text{ mm/s}$ to $V_s = 100 \text{ mm/s}$).

For scanning speeds higher than 150 mm/s (S-III), a relevant increase in the contact angle values takes place. This is especially caused by an increase in the compactness of the treated layer, as shown in Figure 11. The increase in V_s results in the development of textures with a higher contact area between the solid and the liquid phase. In order to verify the behavior of the textured surface by increasing the V_s above the established limits in this research, the microgeometry generated at $V_s = 250$ mm/s has been studied, maintaining a tendency to increase the compactness of the surface, as seen in Figure 11, and giving rise to a maximum contact angle of 146.07° .

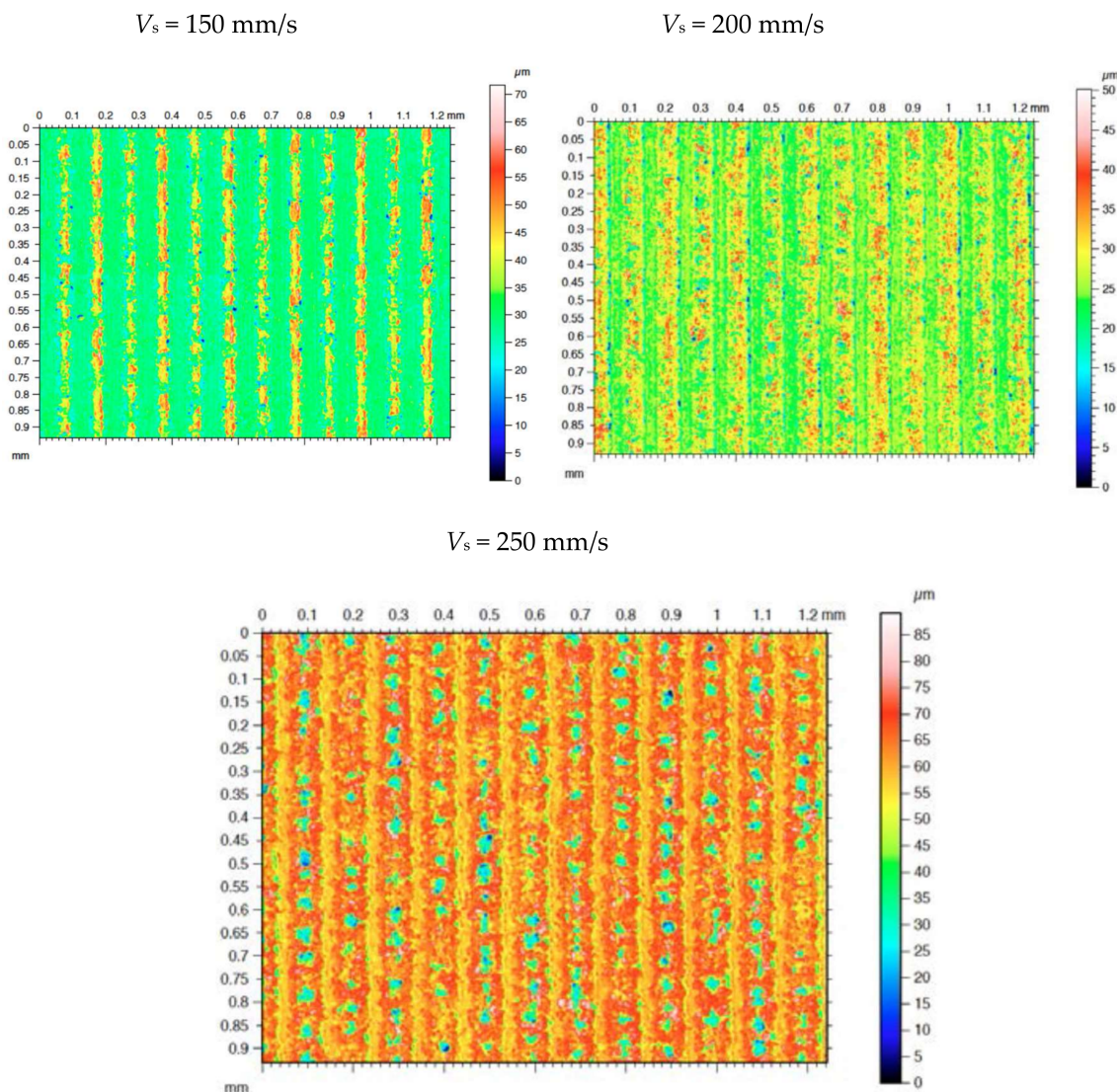


Figure 11. Topographic evolution of the textured layer for S-III speed set, which has the highest scanning speeds ($V_s = 150$ mm/s to $V_s = 200$ mm/s, and $V_s = 250$ mm/s).

In this case, an important dependence cannot be ensured between the results of the contact angle measurement of the textured surface and the r roughness coefficient of the Wenzel model for wetting capacity. This may be due to the lack of homogeneity of the laser-induced topography. In addition, the impossibility of maintaining precise control over the cooling stage, and the solidification of the vaporized material in the process, may produce anomalous behavior regarding the properties of the absorption/repulsion of the liquids of the irradiated surface.

4. Conclusions

The laser texturing process can induce the formation of modified material layers with special topographies for specific applications. Through variations of laser processing parameters, the dimensions and geometry of the texturing tracks can be controlled. The scanning speed of the beam (V_s) is shown to be one of the main variables that govern the laser surface modification in terms of microgeometrical texture generation.

The increase of V_s results in the incidence of less energy on the surface, resulting in a decrease in the roughness parameters (Rz and RSm) that define the maximum dimensions of the texturized grooves. In this aspect, the shape and dimensions of the laser tracks show significant variations as a function of the scanning speed, presenting an evolution from deeper and sharper grooves for lower V_s to semicircular and shallow grooves for higher speeds.

Non-uniform solidification processes are shown to be the main cause of unexpected behavior in the evaluation of wettability. Taking the evaluation of the results obtained as a reference, a dependency relation cannot be ensured between the roughness coefficient r and the contact angle between the liquid and solid phases.

A significant influence has been detected between the pattern and groove depth of the modified layer, and the hydrophobic characteristics of the surface. Likewise, it has been observed that high speeds allow the generation of more defined topographies, giving place to closer parallel structures and increasing the contact area with the liquid phase. This enables the approximation of the contact angle between phases to increase, reaching a maximum of 146.07° for $V_s = 250$ mm/s.

Acknowledgments: This work has received financial support by the Spanish Government (Project DPI2017-84935-R), the European Union (FEDER/FSE) and the Andalusian Government (PAIDI).

Author Contributions: Juan Manuel Vazquez-Martinez, Jorge Salguero Gomez and Moises Batista Ponce conceived and designed the experiments; Juan Manuel Vazquez-Martinez, Pedro Francisco Mayuet Ares, Severo Raul Fernandez-Vidal and Pedro Francisco Mayuet Ares performed the experiments; Juan Manuel Vazquez-Martinez, Pedro Francisco Mayuet Ares and Jorge Salguero Gomez analyzed the data; Juan Manuel Vazquez-Martinez, wrote the paper.

Conflicts of Interest: The authors declare no conflict of interest.

References

1. Cho, J.S.; Beag, Y.; Han, S.; Kim, K.; Cho, J.; Koh, S. Hydrophilic surface formation on materials and its applications. *Surface Coat. Technol.* **2000**, *128*, 66–70. [[CrossRef](#)]
2. Bormashenko, E. Progress in understanding wetting transitions on rough surfaces. *Adv. Colloid Interface Sci.* **2015**, *222*, 92–103. [[CrossRef](#)] [[PubMed](#)]
3. Vazirinasab, E.; Jafari, R.; Momen, G. Application of superhydrophobic coatings as a corrosion barrier: A review. *Surface Coat. Technol.* **2017**, *341*, 40–56. [[CrossRef](#)]
4. Otitoju, T.A.; Ahmad, A.L.; Ooi, B.S. Superhydrophilic (superwetting) surfaces: A review on fabrication and application. *J. Ind. Eng. Chem.* **2017**, *47*, 19–40. [[CrossRef](#)]
5. Belhadjamor, M.; Belghith, S.; Mezlini, S.; El Mansori, M. Effect of the surface texturing scale on the self-clean function: Correlation between mechanical response and wetting behavior. *Tribol. Int.* **2017**, *111*, 91–99. [[CrossRef](#)]
6. Mortazavi, V.; Khonsari, M.M. On the degradation of superhydrophobic surfaces: A review. *Wear* **2017**, *372–373*, 145–157. [[CrossRef](#)]
7. Wojciechowski, L.; Kubiak, K.J.; Mathia, T.G. Roughness and wettability of surfaces in boundary lubricated scuffing wear. *Tribol. Int.* **2016**, *93B*, 593–601. [[CrossRef](#)]
8. Liang, Y.; Shu, L.; Natsu, W.; He, F. Anisotropic wetting characteristics versus roughness on machined surfaces of hydrophilic and hydrophobic materials. *Appl. Surface Sci.* **2015**, *331*, 41–49. [[CrossRef](#)]
9. May, A.; Agarwal, N.; Lee, J.; Lambert, M.; Akkan, C.K.; Nothdurft, F.P.; Aktas, O.C. Laser anisotropic wetting on Ti-6Al-4V surfaces. *Mater. Lett.* **2015**, *138*, 21–24. [[CrossRef](#)]
10. Drelich, J.; Chibowski, E.; Meng, D.D.; Terpilowski, K. Hydrophilic and superhydrophilic surfaces and materials. *Soft Matter* **2011**, *7*, 9804–9829. [[CrossRef](#)]

11. Luo, Y.; Ge, S.; Jin, Z. Wettability Modification for biosurface of titanium alloy by means of sequential carburization. *J. Bionic Eng.* **2009**, *6*, 219–223. [[CrossRef](#)]
12. Pou, P.; Riveiro, A.; del Val, J.; Comesaña, R.; Penide, J.; Arias-González, F.; Soto, R.; Lusquiños, F.; Pou, J. Laser surface texturing of Titanium for bioengineering applications. *Procedia Manuf.* **2017**, *13*, 694–701. [[CrossRef](#)]
13. Shin, S.; Seo, J.; Han, H.; Kang, S.; Kim, H.; Lee, T. Bio-inspired extreme wetting surfaces for biomedical applications. *Materials* **2016**, *9*, 116. [[CrossRef](#)] [[PubMed](#)]
14. Tian, Y.S.; Chen, C.Z.; Li, S.T.; Huo, Q.H. Research progress on laser surface modification of titanium alloys. *Appl. Surface Sci.* **2005**, *242*, 177–184. [[CrossRef](#)]
15. Mohammed, M.T.; Khan, Z.A.; Siddiquee, A.N. Surface modification of titanium materials for developing corrosion behavior in human body environment: A review. *Procedia Mater. Sci.* **2014**, *6*, 1610–1618. [[CrossRef](#)]
16. Vazquez-Martinez, J.M.; Salguero, J.; Botana, F.J.; Gomez-Parra, A.; Fernandez-Vidal, S.R.; Marcos, M. Tribological wear analysis of laser surface treated Ti6Al4V based on volume lost evaluation. *Key Eng. Mater.* **2014**, *615*, 82–87. [[CrossRef](#)]
17. Vazquez-Martinez, J.M.; Salguero, J.; Botana, F.J.; Contreras, J.P.; Fernandez-Vidal, S.R.; Marcos, M. Metrological evaluation of the tribological behavior of laser surface treated Ti6Al4V alloy. *Procedia Eng.* **2013**, *63*, 752–760. [[CrossRef](#)]
18. Leuders, S.; Thone, M.; Riemer, A.; Niendorf, T.; Troster, T.; Richard, H.A.; Maier, H.J. On the mechanical behavior of titanium alloy Ti6Al4V manufactured by selective laser melting: Fatigue resistance and crack growth performance. *Int. J. Fatigue* **2013**, *48*, 300–307. [[CrossRef](#)]
19. Arizmendi, M.; Campa, F.J.; Fernandez, J.; López de Lacalle, L.N.; Gil, A.; Bilbao, E.; Veiga, F.; Lamikiz, A. Model for surface topography prediction in peripheral milling considering tool vibration. *CIRP Ann. Manuf. Technol.* **2009**, *58*, 93–96. [[CrossRef](#)]
20. Komolafe, B.; Mostafa, A. Wetting and spreading behavior of Ti-based brazing filler on Ti64 substrate. *Mater. Res. Express* **2017**, *6*, 066503. [[CrossRef](#)]
21. Vázquez Martínez, J.M.; Salguero Gómez, J.; Batista Ponce, M.; Botana Pedemonte, F.J. Effects of laser processing parameters on texturized layer development and surface features of Ti6Al4V alloy samples. *Coatings* **2018**, *8*, 6. [[CrossRef](#)]
22. Al-Sayed Ali, S.R.; Hussein, A.H.A.; Nofal, A.A.M.S.; Hasseb Elnaby, S.E.I.; Elgazzar, H.A.; Sabour, H.A. Laser powder cladding of Ti-6Al-4V α/β alloy. *Materials* **2017**, *10*, 1178. [[CrossRef](#)] [[PubMed](#)]
23. Martínez, J.M.V.; Pedemonte, F.J.B.; Galvin, M.B.; Gomez, J.S.; Barcena, M.M. Sliding wear behavior of UNS R56400 titanium alloy samples thermally oxidized by laser. *Materials* **2017**, *10*, 830. [[CrossRef](#)] [[PubMed](#)]
24. Wang, D.; Wang, Y.; Wu, S.; Lin, H.; Yang, Y.; Fan, S.; Gu, C.; Wang, J.; Song, C. Customized a Ti6Al4V bone plate for complex pelvic fracture by selective laser melting. *Materials* **2017**, *10*, 35. [[CrossRef](#)] [[PubMed](#)]
25. Lopez de Lacalle, L.N.; Rodríguez, A.; Lamikiz, A.; Celaya, A.; Alberdi, R. Five-axis machining and burnishing of complex parts for the improvement of surface roughness. *Mater. Manufact. Process.* **2011**, *26*, 997–1003. [[CrossRef](#)]
26. Palmieri, F.L.; Wohl, C.J. *Topographical Modification of Polymers and Metals by Laser Ablation to Create Superhydrophobic Surfaces in: Laser Technology: Applications in Adhesion and and Related Areas*; Milttal, K.L., Lei, W.-S., Eds.; Scrivner Publishing: Beverly, MA, USA, 2018.
27. Amrei, M.M.; Davoudi, M.; Chase, G.G.; Vahedi Tafreshi, V. Effects of roughness on droplet apparent contact angles on a fiber. *Separ. Purif. Technol.* **2017**, *180*, 107–113. [[CrossRef](#)]
28. Karim, A.M.; Rothstein, J.P.; Kavehpour, H.P. Experimental study of dynamic contact angles on rough hydrophobic surfaces. *J. Colloid Interface Sci.* **2018**, *513*, 658–665. [[CrossRef](#)] [[PubMed](#)]
29. Bormashenko, E. General equation describing wetting of rough surfaces. *J. Colloid Interface Sci.* **2011**, *360*, 317–319. [[CrossRef](#)] [[PubMed](#)]
30. Kubiak, K.J.; Wilson, M.C.T.; Mathia, T.G.; Carval, P. Wettability versus roughness of engineering surfaces. *Wear* **2011**, *3–4*, 523–528. [[CrossRef](#)]
31. Belaud, V.; Valette, S.; Stremstoerfer, G.; Bigerelle, M.; Benayoun, S. Wettability versus roughness: Multi-scales approach. *Tribol. Int.* **2015**, *82 Pt B*, 343–349. [[CrossRef](#)]
32. Raimbault, O.; Benayoun, S.; Anselme, K.; Maclairb, C.; Bourgade, T.; Kietzig, A.M.; Girard-Lauriault, P.L.; Valette, S.; Donnet, C. The effects of femtosecond laser-textured Ti-6Al-4V on wettability and cell response. *Mater. Sci. Eng. C* **2016**, *69*, 311–320. [[CrossRef](#)] [[PubMed](#)]

33. ISO 25178-2 Geometrical Product Specifications (GPS). *Surface Texture: Areal—Part 2, Terms, Definitions and Surface Texture Parameters*; International Organization Standardization (ISO): Geneva, Switzerland, 2012.
34. ISO 4287 Geometrical Product Specifications (GPS). *Surface Texture: Profile Method—Terms, Definitions and Surface Texture Parameters*; International Organization Standardization (ISO): Geneva, Switzerland, 1997.
35. Peltonen, J.; Järn, M.; Areva, S.; Linden, M.; Rosenholm, J.B. Topographical Parameters for specifying a three-dimensional surface. *Langmuir* **2004**, *20*, 9428–9431. [[CrossRef](#)] [[PubMed](#)]



© 2018 by the authors. Licensee MDPI, Basel, Switzerland. This article is an open access article distributed under the terms and conditions of the Creative Commons Attribution (CC BY) license (<http://creativecommons.org/licenses/by/4.0/>).